A shared threat-anticipation circuit is dynamically engaged at different moments by certain and uncertain threat

Brian R. Cornwell[1]
Paige R. Didier[2]
Shannon E. Grogans[2]
Allegra S. Anderson[5]
Samiha Islam[6]
Hyung Cho Kim[2,3]
Manuel Kuhn[7]
Rachael M. Tillman[8]
Juyoen Hur[9]
Zachary S. Scott[2]
Andrew S. Fox[10,11]
Kathryn A. DeYoung[2]
Jason F. Smith[2] *
Alexander J. Shackman[2,3,4] *

[1]Department of Psychological & Brain Sciences, George Washington University, Washington, DC 20006 USA. Department of [2]Psychology; [3]Neuroscience and Cognitive Science Program; and [4]Maryland Neuroimaging Center, University of Maryland, College Park, MD 20742 USA. [5]Department of Psychiatry and Human Behavior, Brown University, Providence, RI 02912 USA. [6]Department of Psychology, University of Pennsylvania, Philadelphia, PA USA. [7]Center for Depression, Anxiety and Stress Research, McLean Hospital, Harvard Medical School, Belmont, MA 02478 USA. [8]McGill Neuropsychology, Bethesda, MD 20814 USA. [9]Department of Psychology, Yonsei University, Seoul 03722, Republic of Korea. [10]Department of Psychology and [11]California National Primate Research Center, University of California, Davis, CA 95616 USA.

* contributed equally

Figures: 5
Supplementary Materials: 1 .docx file (supplementary Method and Results)
Key Words: affective neuroscience, fear and anxiety, bed nucleus of the stria terminalis (BST/BNST), central extended amygdala (EAc), Research Domain Criteria (RDoC)

Please address manuscript correspondence to
Alexander J. Shackman (shackman@umd.edu)

ACKNOWLEDGEMENTS

We acknowledge assistance and critical feedback from A. Antonacci, L. Friedman, J. Furcolo, C. Grubb, J. Hassani, R. Hum, C. Kaplan, J. Kuang, M. Kuhn, C. Lejuez, D. Limon, B. Nacewicz, L. Pessoa, S. Rose, J. Swayambunathan, A. Vogel, B. Winters, J. Wedlock, members of the Affective and Translational Neuroscience Laboratory, the staff of the Maryland Neuroimaging Center, and the Office of the Registrar at the University of Maryland. This work was partially supported by the California National Primate Center; National Institutes of Health (AA030042, DA040717, MH107444, MH121409, MH121735, MH128336, MH129851, OD011107, MH131264); National Research Foundation of Korea (2021R1F1A1063385 and 2021S1A5A2A03070229); University of California, Davis; University of Maryland; and Yonsei Signature Research Cluster Program (2021-22-0005). Authors declare no conflicts of interest.

AUTHOR CONTRIBUTIONS

A.J.S., K.A.D., and J.F.S. designed the overall study. J.F.S. envisioned the present project. J.F.S. and A.J.S. developed and optimized the imaging paradigm. K.A.D. managed data collection and study administration. K.A.D., J.F.S., A.S.A, S.I., and R.M.T. collected data. J.F.S. and M.K. developed data processing and analytic software for imaging analyses. J.F.S., J.H., H.C.K., and R.M.T. processed imaging data. J.F.S., B.R.C., and A.J.S. analyzed imaging data. J.F.S., A.J.S., and B.R.C. developed the analytic strategy. B.R.C., P.R.D., J.F.S., A.S.F., and A.J.S. interpreted data. B.R.C., S.G., J.F.S., and A.J.S. wrote the paper. P.R.D., A.J.S., B.R.C., J.F.S., and Z.S.S. created figures and tables. A.J.S. funded and supervised all aspects of the study. All authors contributed to reviewing and revising the paper and approved the final version.

RESOURCE SHARING

Raw data are available at the National Institute of Mental Health Data Archive (https://nda.nih.gov/edit_collection.html?id=2447). Neuroimaging maps are available at NeuroVault (https://neurovault.org/collections/15274). Task materials, statistical code, and de-identified processed data are available at OSF (https://osf.io/e2ngf). The negative affect brain signature is available at Github (https://github.com/canlab/Neuroimaging_Pattern_Masks/tree/master/Multivariate_signature_patterns/2021_Ceko_MPA2_multiaversive).

ABSTRACT (149/150)

Temporal dynamics play a central role in models of emotion: *"fear"* is widely conceptualized as a phasic response to certain-and-imminent danger, whereas *"anxiety"* is a sustained response to uncertain-or-distal harm. Yet the underlying human neurobiology remains contentious. Leveraging an ethnoracially diverse sample, translationally relevant paradigm, and theory-driven modeling approach, we demonstrate that certain and uncertain threat recruit a shared threat-anticipation circuit. This circuit exhibits persistently elevated activation when anticipating uncertain threat encounters and a transient burst of activation in the moments before certain encounters. For many scientists and clinicians, feelings are the defining feature of human fear and anxiety. Here we used an independently validated brain signature to covertly decode the momentary dynamics of anticipatory distress for the first time. Results mirrored the dynamics of neural activation. These observations provide fresh insights into the neurobiology of threat-elicited emotions and set the stage for more ambitious clinical and mechanistic research.

INTRODUCTION

Fear and anxiety are evolutionarily conserved features of mammalian life that help protect us from harm[1]. But when expressed too strongly or pervasively, they can be crippling[2, 3]. Anxiety-related disorders impose a staggering burden on global public health, afflicting ~360 million individuals annually[4, 5]. In the U.S. alone, ~1 in 3 individuals will experience a lifetime disorder, service utilization is surging, and annual healthcare costs exceed $40B, drawing the attention of the U.S. Surgeon General, White House, and other policymakers[6-11]. Existing treatments were developed decades ago and have limited effectiveness, durability, and tolerability, underscoring the need to clarify the underlying neurobiology[12-15].

Temporal dynamics play a central role in conceptual models of emotion, with many theorists and clinicians conceptualizing *"fear"* as a phasic response to certain-and-imminent danger and *"anxiety"* as a sustained response to uncertain-or-distal harm[1, 16-23]. Work harnessing the millisecond resolution of psychophysiological measures supports this view, showing that defensive behaviors exhibit specific temporal patterns across different threat contexts[20, 24-30]. When the timing of threat encounters is uncertain, a sustained state of heightened reactivity is evident. In contrast, when encounters are certain and imminent, a transient burst of heightened defensive responding is triggered. Longer threat cues, with explicit 'count-down' signals, elicit more complex dynamics, marked by a rapid initial rise in defensive responding, followed by a sustained level of elevated reactivity during the intermediate period, and a phasic surge just prior to the threat encounter.

Human neuroimaging studies have begun to reveal the broad contours of the neural circuitry recruited by certain and uncertain threat[31], but have yet to plumb the moment-by-moment neural dynamics anticipated by theory and psychophysiological research. Most fMRI studies have relied on oversimplified 'boxcar' modeling approaches that assume static, time-invariant neural responses to anticipated threat encounters. We and others have begun to explore finer-grained models for descriptive purposes, but have yet to use

them for rigorous hypothesis testing[32, 33]. Consequently, it remains unclear whether phasic (*"fear"*) and sustained (*"anxiety"*) neural responses to threat are segregated into dissociable anatomical systems, as some have posited[1, 16, 22, 34-40], or are co-localized to a singular system that shows distinctive activation dynamics across different threat contexts, as we have hypothesized[31, 32, 41, 42].

To address this fundamental question, we used a novel combination of fMRI techniques—including theory-driven hemodynamic modeling, focused region-of-interest (ROI) analyses, and multivoxel brain signature analyses—to interrogate the moment-by-moment dynamics of threat-elicited neural activity and subjective distress in 220 ethnoracially diverse participants. Data were collected using the Maryland Threat Countdown (MTC), a well-established paradigm for manipulating the temporal certainty of threat encounters (**Figure 1a**)[32, 43-45]. The MTC is an fMRI-optimized variant of threat assays that have been pharmacologically and psychophysiologically validated in rodents[46-48] and humans[25], maximizing translational relevance. Prior work focused on this and other samples demonstrates that this paradigm robustly increases subjective symptoms of distress and objective signs of arousal, reinforcing its validity as an experimental probe of human fear and anxiety (**Supplementary Figure S1**)[32, 43-45].

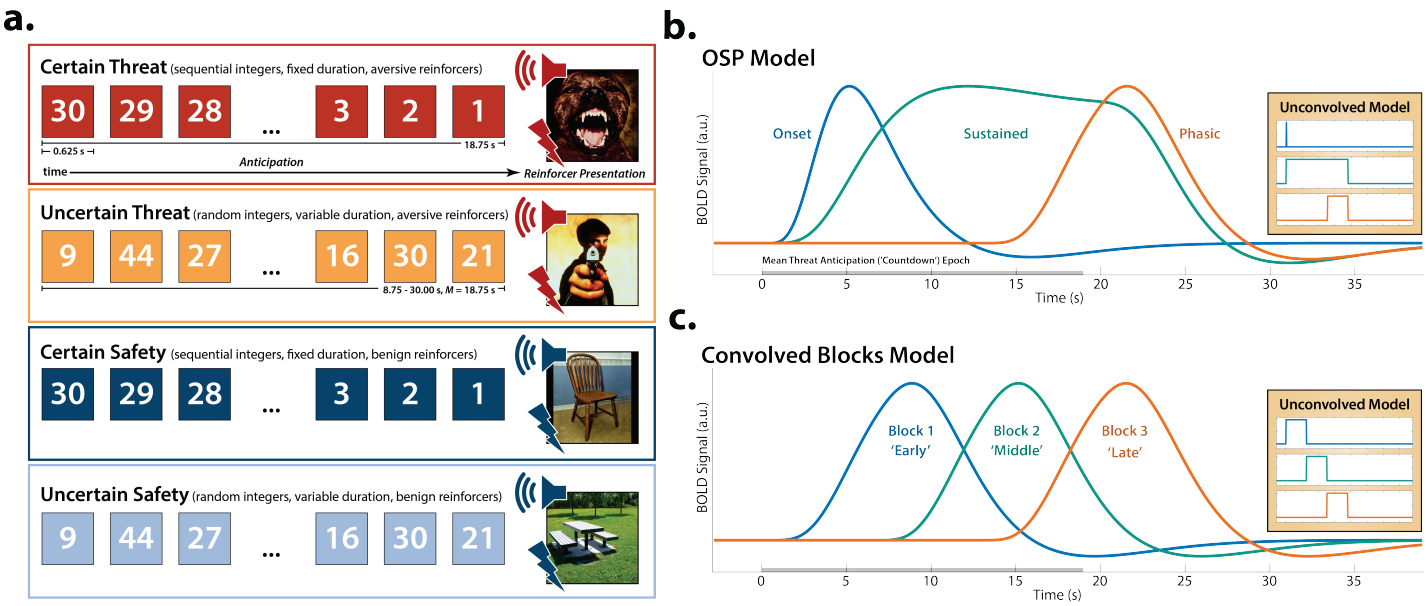

Figure 1. Conceptual overview. a. *Threat-anticipation paradigm.* The Maryland Threat Countdown (MTC) takes the form of a 2 (*Valence:* Threat, Safety) × 2 (*Temporal Certainty:* Certain, Uncertain) randomized event-related design. On certain-threat trials, participants saw a descending stream of integers or 'countdown' for 18.75 s. To ensure robust fear and anxiety, this period of anticipation always terminated with the presentation of a noxious electric shock, unpleasant picture, and thematically related audio clip (e.g., scream). Uncertain-threat trials were similar, but the integer stream was randomized and presented for an uncertain and variable duration (8.75-30.00 s; *M*=18.75 s). Here, participants knew that something aversive was going to occur, but they had no way of knowing precisely when. Safety trials were similar but terminated with the delivery of neutral reinforcers (e.g., just-perceptible electrical stimulation). **b. *OSP model.*** Prior research has relied on oversimplified 'boxcar' modeling approaches that reduce anticipatory neural dynamics to a single average response[49]. Here, we used two complementary hemodynamic modeling approaches to interrogate time-varying responses to certain and uncertain threat. The OSP model used multiple-regression to identify the variance in threat-anticipation signals uniquely associated with temporally overlapping Onset, Sustained, and Phasic regressors. The design matrix incorporated a punctate event time-locked to the onset of the anticipation epoch, a variable-duration rectangular function spanning the entirety of the anticipation epoch (to capture sustained increases in activation), and a temporally overlapping rectangular function time-locked to the offset of the anticipation epoch (to capture phasic surges in activation to acute threat). Note that conventional boxcar models are equivalent to the green signal. **c. *Convolved Blocks Model.*** To clarify interpretation, we employed a piecewise model that splits the anticipation epoch into a sequence of short (6.25 s), non-overlapping rectangular functions ('blocks'), each convolved with a canonical hemodynamic response function. While arbitrary in timing, the Convolved Blocks model yields activation estimates that are independent, inferentially intuitive, and statistically comparable across time, enabling us to more fully assess apparent surges in activation in the moments just before certain-threat encounters. Abbreviations—a.u., arbitrary units; BOLD, blood-oxygenation-level-dependent; HRF, hemodynamic response function; OSP, Onset-Sustained-Phasic; s, seconds.

Supplementary Figure S1. The Maryland Threat Countdown paradigm is a valid experimental probe of anticipatory fear and anxiety. Participants were periodically prompted to rate the intensity of fear/anxiety during the anticipation ('countdown') period of the prior trial, using a 1 (*minimal*) to 4 (*maximal*) scale (16.7% trials). Skin conductance was continuously acquired throughout. As detailed elsewhere, we used a series of repeated-measures GLMs to confirm that the threat-anticipation paradigm had the intended impact on subjective symptoms of distress and objective signs of arousal [43]. **a. *Threat anticipation evokes subjective distress.*** Participants Fearful and anxious feelings were significantly elevated during the anticipation of Threat compared to Safety, and this was particularly evident when threat encounters were uncertain in their timing (*Valence:* $F(1,219)=1{,}108.5$, $p<0.001$; *Certainty:* $F(1,219)=208.4$, $p<0.001$; *Valence × Certainty:* $F(1,219)=31.9$, $p<0.001$; *Threat, Uncertain vs. Certain:* $F(1,219)=148.5$, $p<0.001$; *Safety, Uncertain vs. Certain:* $F(1,219)=76.6$, $p<0.001$). **b. *Threat anticipation evokes objective signs of arousal.*** A similar pattern was evident for skin conductance level, an objective psychophysiological index of arousal (*Valence:* $F(1,217)=792.79$, $p<0.001$; *Certainty:* $F(1,217)=139.6$, $p<0.001$; *Valence × Certainty:* $F(1,217)=664.4$, $p<0.001$; *Threat, Uncertain vs. Certain:* $F(1,217)=457.8$, $p<0.001$; *Safety, Uncertain vs. Certain:* $F(1,217)=271.2$, $p<0.001$). Two participants were excluded from skin-conductance analyses due to insufficient usable data. Taken together, these observations confirm the validity of the Maryland Threat Countdown as an experimental probe of fear and anxiety, replicating prior work in community volunteers [45]. Bars indicate the means (*colored bars*), Bayesian 95% highest density intervals (HDI; *gray bands*), and individual participants (*gray dots*).

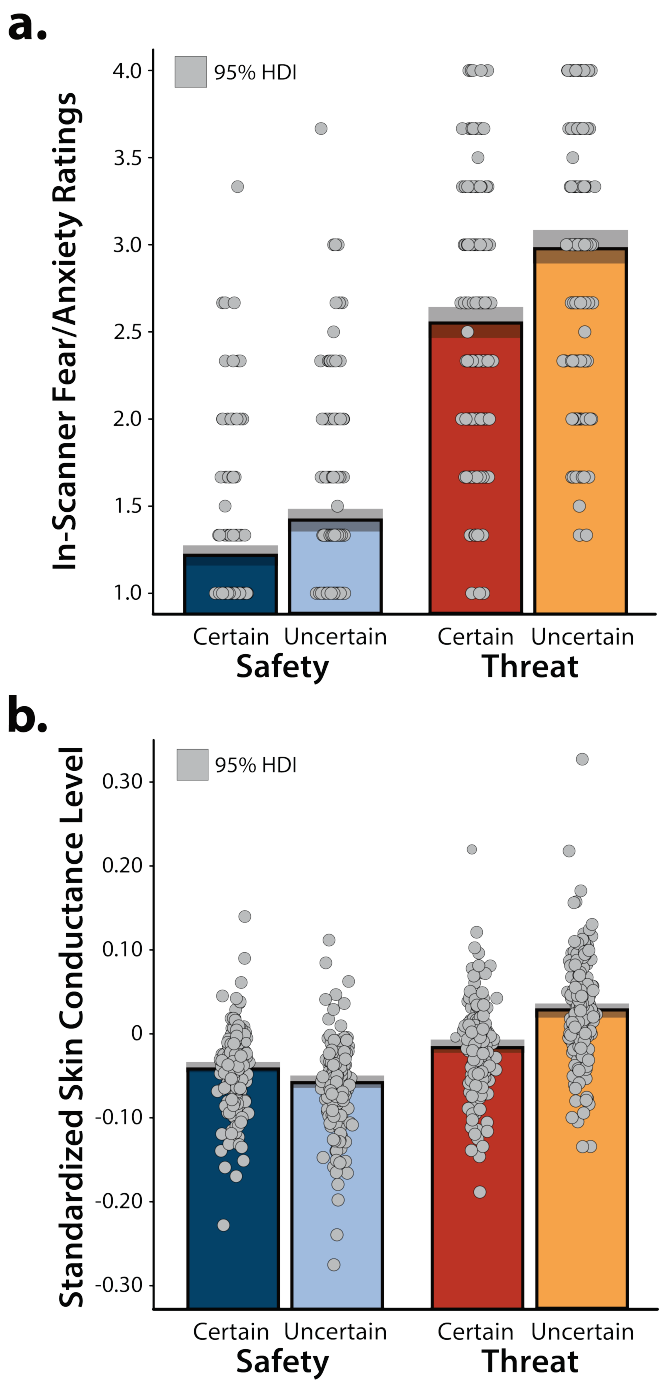

207 **RESULTS**

208 **Conventional 'boxcar' modeling reveals a shared threat-anticipation circuit**

209 The present sample of 220 datasets represents a superset of the 99 featured in an earlier report that relied
210 on a conventional 'boxcar' modeling approach, older data-processing pipeline, and coarser spatial-
211 smoothing kernel (6-mm)[32]. Here we used standard voxelwise GLMs to confirm that conventional
212 modeling of the larger reprocessed dataset broadly reproduced our published results. As expected, results
213 revealed significant activation during periods of uncertain-threat anticipation, both in subcortical regions
214 implicated in rodent models of fear and anxiety—such as the periaqueductal gray (PAG), bed nucleus of
215 the stria terminalis (BST), and dorsal amygdala—and in frontocortical regions that are especially well-
216 developed in humans—including the midcingulate cortex (MCC), anterior insula/frontal operculum
217 (AI/FrO), and rostral dorsolateral prefrontal cortex (dlPFC; FDR $q<0.05$, whole-brain corrected;
218 **Supplementary Figure S2** and **Supplementary Tables S1-S5**). The same pattern was evident during
219 certain-threat anticipation, with overlapping voxels across threat contexts in each of these key regions. In
220 short, when viewed through the macroscopic lens of conventional fMRI modeling, uncertain- and certain-
221 threat anticipation engage overlapping neural circuits, suggesting a common neural substrate in humans.

222
223

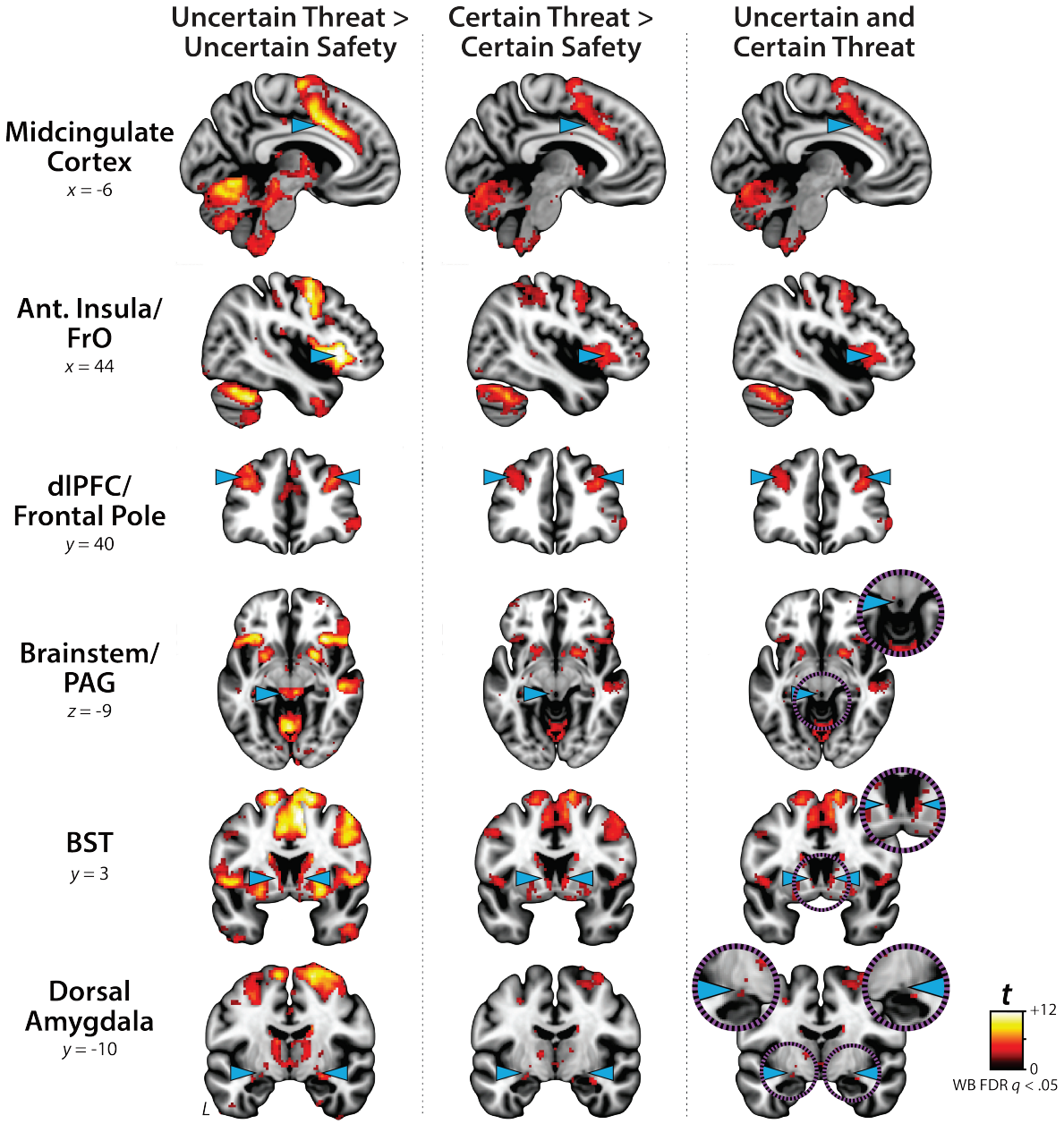

Supplementary Figure S2. Uncertain- and certain-threat anticipation recruit a shared cortico-subcortical circuit. To facilitate comparison with prior work, we computed a conventional 'boxcar' analysis, which models the anticipation epoch ('countdown') as a single average response. As shown in the *left column*, uncertain-threat anticipation was associated with significant activation across a widely distributed network of regions previously implicated in the expression and regulation of human fear and anxiety (FDR q<.05, whole-brain corrected) [31]. As shown in the *middle column*, similar results were evident for certain-threat anticipation. In fact, as shown in the right column, a minimum-conjunction analysis [50] (Logical 'AND' of the 2 thresholded contrasts) confirmed voxelwise co-localization in each of these key regions. These observations replicate prior work in university and community samples, confirm that our paradigm robustly engages the canonical threat-anticipation circuit, and set the stage for detailed analyses of more complex neural dynamics [32, 42, 43, 45]. Note. To enhance neuroanatomical resolution, these analyses leveraged a smaller spatial-smoothing kernel (4-mm) than prior work by our group (6-mm). Abbreviations—Ant., anterior; BST, bed nucleus of the stria terminalis; dlPFC, dorsolateral prefrontal cortex; FDR, false discovery rate; FrO, frontal operculum; L, left; PAG, periaqueductal gray; t, Student's *t*-test; WB, whole-brain corrected.

Sustained activation is evident during the anticipation of both uncertain and certain threat

While useful, conventional hemodynamic models cannot resolve time-varying neural responses to anticipated threat. To address this, we used a multiple-regression framework to transform the observed hemodynamic signal into a weighted linear combination of Onset, Sustained, and Phasic responses (**Figure 1b** and **Supplementary Figure S3**). Standard voxelwise GLMs were then used to identify regions showing sustained activation during the anticipation of uncertain and certain threat (FDR q<0.05, whole-brain corrected). Results closely resembled those yielded by conventional 'boxcar' analyses (**Supplementary Figure S2**), with sustained activation evident throughout the canonical threat-anticipation circuit[31]—including the BST and dorsal amygdala—during the anticipation of uncertain and certain threat (**Figure 2; Supplementary Tables S6-S12**). Despite this qualitative similarity, direct comparison of the two threats indicated that sustained responses were significantly stronger when the timing of threat encounters was uncertain (**Figure 2**).

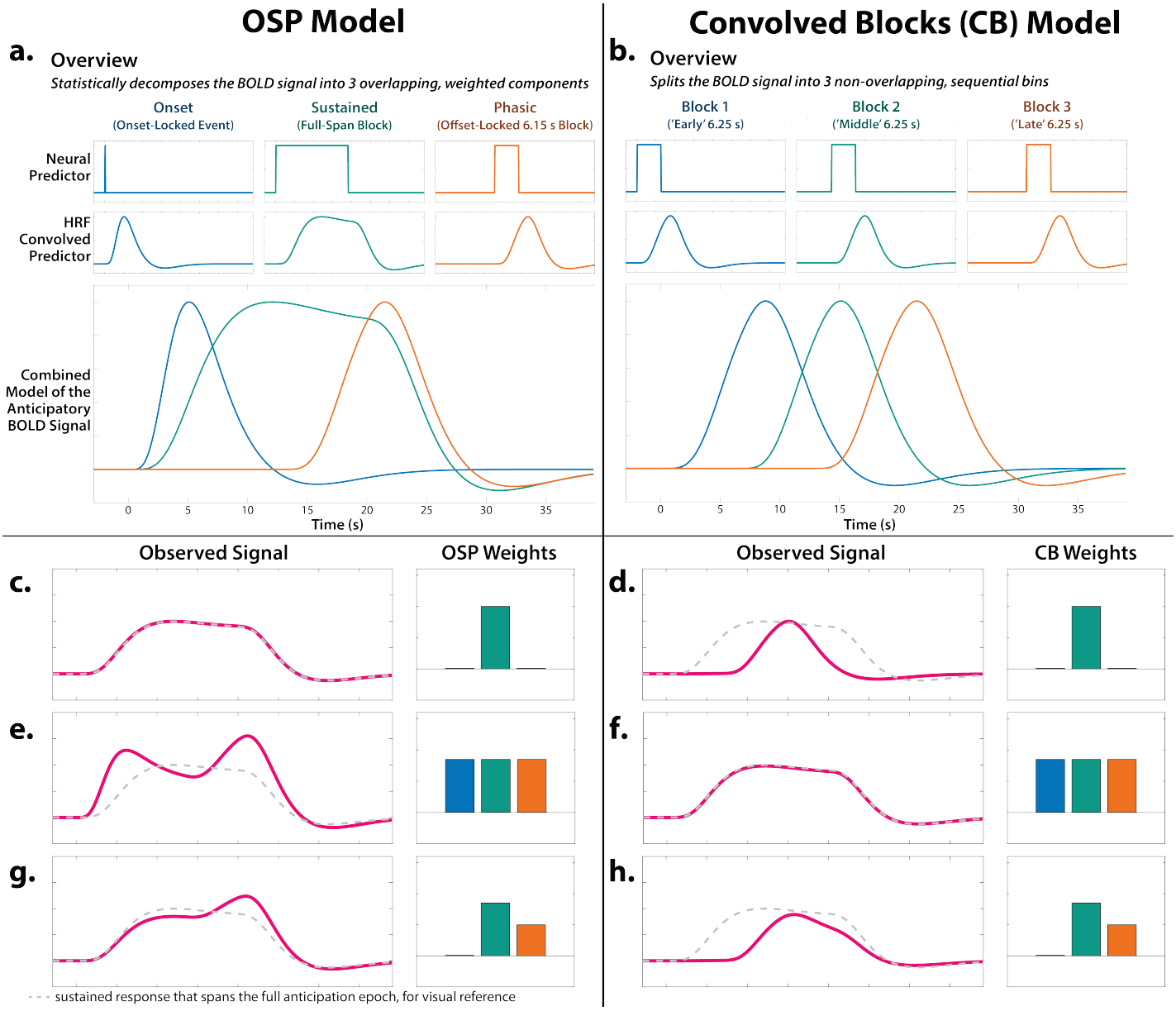

Supplementary Figure S3. Theory-driven hemodynamic modeling. The vast majority of neuroimaging studies have relied on oversimplified 'boxcar' modeling approaches that reduce threat-related activation to a single average response [49]. Here we used two complementary hemodynamic modeling approaches to quantify and statistically interrogate time-varying responses to certain- and uncertain-threat anticipation. Panels ***a*** and ***b*** provide a general overview of the two theory-driven models. Panels ***c-h*** illustrate key interpretive nuances. **a.** ***Overview of the OSP Model.*** The OSP model used multiple-regression to partition the variance in threat-anticipation signals uniquely associated with overlapping Onset, Sustained, and Phasic regressors. The design matrix incorporated a punctate event time-locked to the onset of the anticipation ('countdown') epoch, a variable-duration rectangular function spanning the entirety of the anticipation epoch (to capture sustained increases in activation), and a temporally overlapping rectangular-function time-locked to the *offset* of the anticipation epoch (to capture phasic surges in activation to acute threat, independent of threat certainty or trial duration). This approach provides a unified, non-arbitrary means of addressing the variable duration and timing of uncertain trials (**Figure 1a**). **c.** ***Overview of the Convolved Blocks (CB) Model.*** To clarify interpretation, we employed a piecewise hemodynamic model that arbitrarily splits the anticipation epoch into a sequence of short (6.25 s), non-overlapping rectangular functions ('blocks'), each convolved with a canonical hemodynamic response

function. Hypothesis testing focused on the first three blocks, corresponding to the average duration of certain-and uncertain-threat anticipation (cf. **Figure 1a**). While arbitrary in timing, the Convolved Blocks model yields activation estimates that are independent, intuitive, and statistically comparable across time, making it possible to more completely assess apparent surges in activation in the moments just prior to certain-threat encounters. **c.** Consider a voxel that shows a sustained level of heightened activation during the certain anticipation of threat (*red*). In the OSP model, this is captured by a strong loading or 'weight' on the Sustained regressor and nil loadings on the Onset and Phasic regressors. **d.** In the CB model, the same pattern of weights is instead associated with a transient increase in hemodynamic signal in the middle of the anticipation epoch. **f.** In the CB model, sustained activation is captured by uniformly strong loadings across the early, middle, and late regressors. **e.** In the OSP model, this pattern of weights is associated with transient onset and phasic responses, superimposed on a large sustained response. In effect, the Onset and Phasic regressors serve to modulate the leading and trailing edges of a sustained wave of activation. It also merits comment that, although the three regression weights are equally strong ($O \approx S \approx P$), the momentary height of the hemodynamic signal is not ($O > S < P$). This reflects the fact that the OSP model casts the threat-anticipation signal as the linear combination of 3 temporally overlapping regressors. **g.** Likewise, in the OSP model the relative height of activation ($S < P$) can be reversed from the rank order of the fitted regression weights ($S > P$). **h.** In contrast, the CB model provides a one-to-one mapping between the momentary height of the observed hemodynamic signal and the early, middle, and late regression weights, enabling straightforward statistical comparisons across moments in time. Abbreviations—BOLD, blood-oxygenation-level-dependent; CB, Convolved Blocks model; HRF, hemodynamic response function; OSP, Onset-Sustained-Phasic; s, seconds.

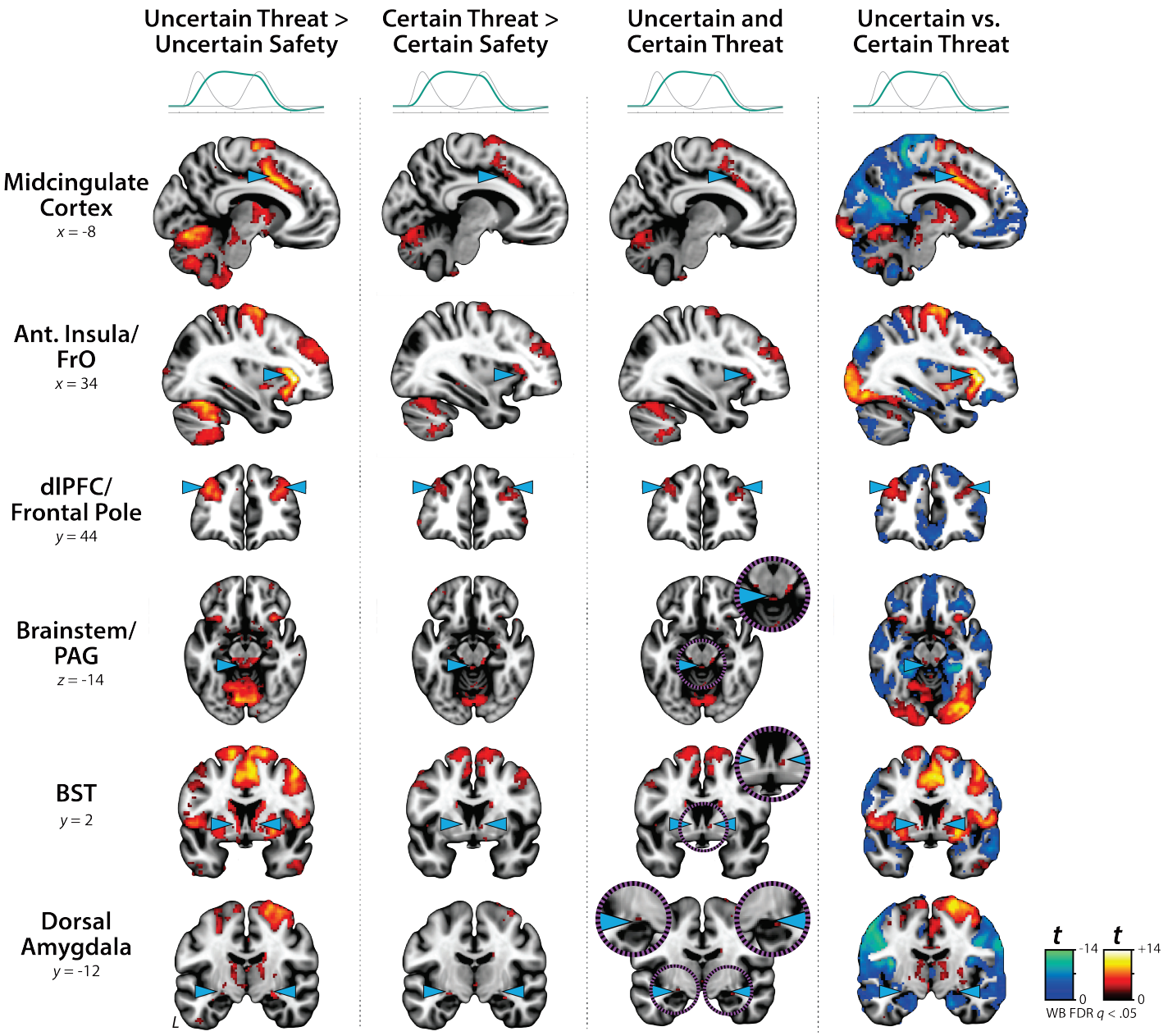

Figure 2. Sustained activation is evident during uncertain- and certain-threat anticipation. Key regions showing evidence of sustained hemodynamic activity during the anticipation of temporally uncertain threat (*first column*) and certain threat (*second column*) compared to their respective control conditions (FDR q<0.05, whole-brain corrected). A minimum-conjunction[50] (logical 'AND') of the two contrasts revealed colocalization throughout the threat-anticipation circuit (*third column*). A direct contrast of the two contexts indicated that sustained signals were more pronounced during uncertain-threat anticipation (*fourth column*). Note: 4-mm smoothing kernel. Abbreviations—Ant., anterior; BST, bed nucleus of the stria terminalis; dlPFC, dorsolateral prefrontal cortex; FDR, false discovery rate; FrO, frontal operculum; L, left; PAG, periaqueductal gray; t, Student's *t*-test; vs., versus; WB, whole-brain corrected.

327 **Phasic responses to certain-and-imminent threat are evident in the same regions that show**
328 **sustained responses to uncertain threat, indicating a shared threat-anticipation circuit**

329 Emotion theory and psychophysiological research suggest that defensive responses surge in the moments
330 just before certain encounters with threat, but the underlying human neurobiology has remained unclear.
331 Here we used a voxelwise GLM focused on the Phasic component of the OSP model—which is time-locked
332 to the *offset* of the anticipation epoch, regardless of duration or threat certainty—to identify regions
333 showing significantly increased activation to certain-and-imminent threat (FDR q<0.05, whole-brain
334 corrected; **Supplementary Figure S3**). Results revealed robust phasic responses during the terminal
335 portion of certain-threat anticipation in every key region, including the BST and right dorsal amygdala
336 (**Figure 3**, *left column*). As expected, phasic responses were notably weaker (e.g., midcingulate) or
337 nonsignificant (e.g., BST) in the corresponding moments of uncertain-threat anticipation, when threat
338 imminence is unknown to participants (**Figure 3**, *middle columns*). Visual inspection of the results suggests
339 that the regions showing phasic responses to certain-and-imminent threat recapitulate those showing
340 sustained responses during uncertain-threat anticipation (**Figure 2**). Consistent with this impression, a
341 minimum-conjunction[50] (logical 'AND') of the two contrasts revealed voxelwise overlap in all regions
342 (**Figure 3**, *right column*). The noteworthy degree of co-localization suggests that both kinds of threat
343 recruit a shared threat-anticipation circuit that exhibits context-specific dynamics: sustained levels of
344 heightened activation when threat encounters are uncertain and distal, and phasic surges in activation
345 when threat encounters are certain and imminent (**Supplementary Tables S13-S19**). Furthermore,
346 because both conditions ultimately culminate in threat encounters (**Figure 1a**), the absence of robust
347 hemodynamic responses to uncertain threat indicates that phasic recruitment of the threat-anticipation
348 circuit to acute threat is not an artifact of reinforcer (e.g., shock) delivery.
349

While not the focus of the present report, exploratory analyses of the OSP Onset regressor (**Figure 1b**) revealed significant responses to both certain- and uncertain-threat anticipation in the right dorsal amygdala in the region of the basal and cortical nuclei, consistent with an attentional orienting or salience detection function (**Supplementary Figure S4** and **Supplementary Tables S20-S24**)[51, 52].

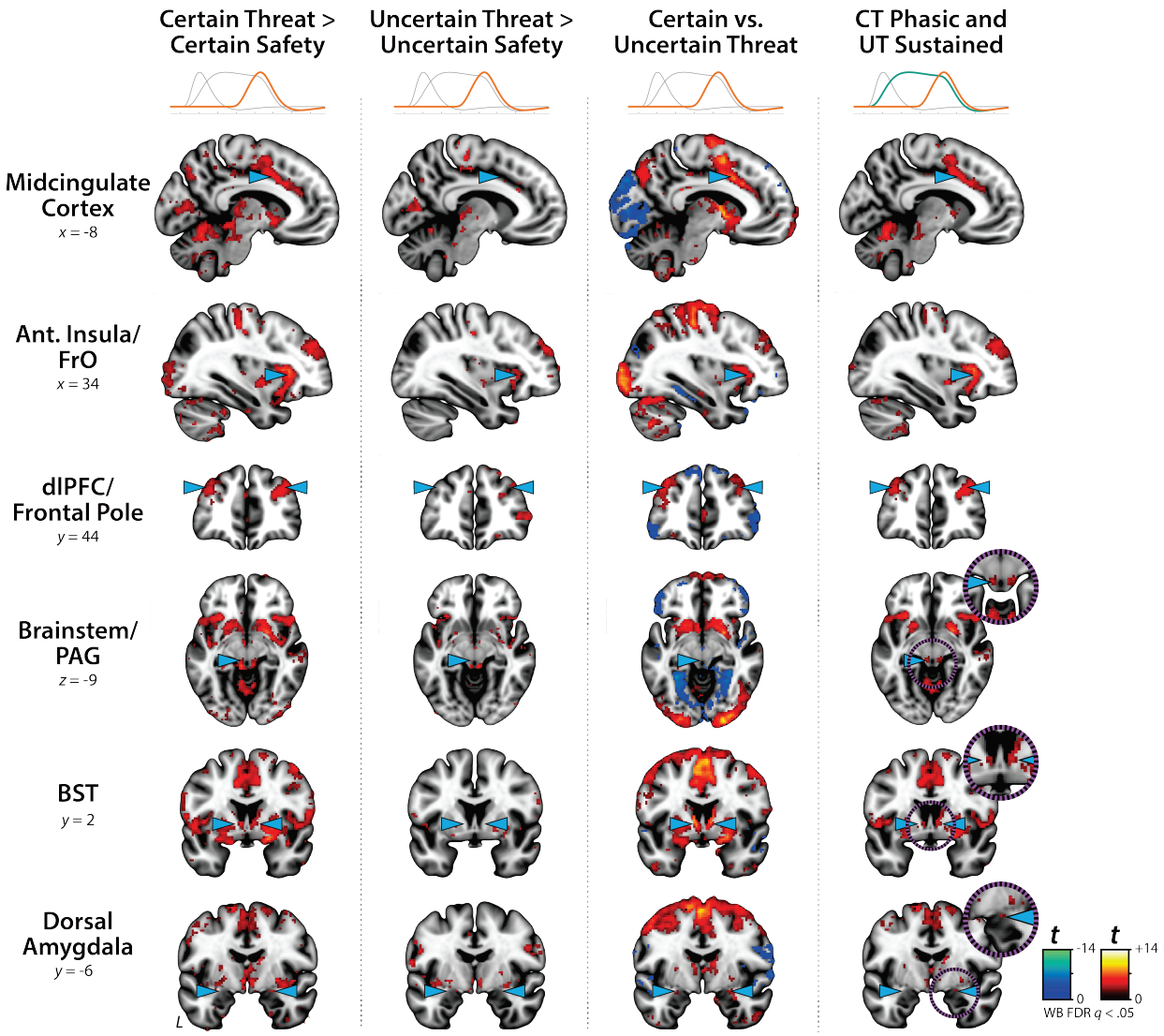

Figure 3. Phasic responses to certain-and-imminent threat are evident in the same regions that show sustained responses during the uncertain anticipation of threat. Regions showing significant phasic activation during the final seconds of certain-threat anticipation (*first column*) and uncertain-threat anticipation (*second column*) compared to their respective control conditions (FDR q<0.05, whole-brain corrected). With the exception of the PAG, every key region showed significantly stronger phasic responses to certain threat (*third column*). Visual inspection suggests that the regions showing phasic responses to certain-and-imminent threat (*first column*) largely recapitulate the circuit showing sustained responses to uncertain-threat anticipation (**Figure 2**). Indeed, a minimum-conjunction[50] (logical 'AND') of the two thresholded contrasts revealed voxelwise overlap in all regions (*fourth column*), suggesting that certain and uncertain threat are anatomically colocalized in a shared threat-anticipation circuit. Note: 4-mm smoothing kernel. Abbreviations—Ant., anterior; BST, bed nucleus of the stria terminalis; CT, certain-threat anticipation greater than certain-safety anticipation; dlPFC, dorsolateral prefrontal cortex; FDR, false discovery rate; FrO, frontal operculum; L, left; PAG, periaqueductal gray; t, Student's *t*-test; UT, uncertain-threat anticipation greater than uncertain-safety anticipation; vs., versus; WB, whole-brain corrected.

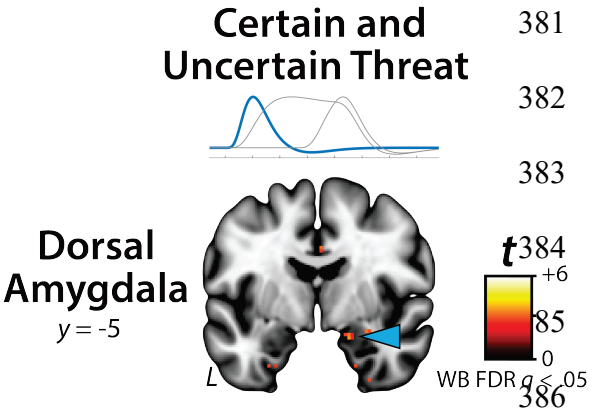

Supplementary Figure S4. The dorsal amygdala is sensitive to the onset of the threat-anticipation epoch, independent of temporal certainty. Exploratory analyses of the OSP Onset regressor revealed significant responses to both certain- and uncertain-threat anticipation in the right dorsal amygdala in the region of the basal and cortical nuclei. Figure depicts the minimum conjunction (logical 'AND') of certain and uncertain threat relative to their respective control conditions (FDR q<0.05, whole-brain corrected). Note: 4-mm smoothing kernel. Abbreviations—FDR, False discovery rate; L, left; t, Student's *t*-test; WB, whole-brain corrected.

399 **Phasic responses to acute threat reflect genuine surges in activation**

400 The OSP Phasic results imply that activation significantly increased from the middle to the end of certain-
401 threat anticipation, and suggest that this difference is more pronounced for certain than uncertain threat.
402 Yet neither inference is licensed by the results, which are focused on *within*-moment statistical contrasts
403 (e.g., *OSP Phasic regressor:* certain vs. uncertain threat). The absence of *between*-moment tests reflects the
404 fact that the partial-regression coefficients yielded by the OSP model do not allow straightforward
405 interpretation of between-moment contrasts (**Supplementary Figure S3**). To sidestep this, follow-up
406 analyses leveraged a second hemodynamic model, which split the anticipation epoch into a sequence of
407 short (6.25 s), non-overlapping blocks (rectangular functions), each convolved with a canonical
408 hemodynamic response function (**Figure 1c**). While arbitrary in timing, this Convolved Blocks model yields
409 activation estimates that are independent, inferentially intuitive, and statistically comparable across
410 moments in time (**Supplementary Figure S3**). A standard voxelwise GLM was then used to identify
411 regions showing significant surges in activation during the late relative to the middle portion of certain-
412 threat anticipation (FDR q<0.05, whole-brain corrected). Results revealed significant activation in every
413 key region except for the PAG, with a similar pattern evident for the between-moments comparison of
414 certain to uncertain threat (**Supplementary Figure S5** and **Supplementary Tables S25-S30**). Taken
415 together, these observations indicate that phasic hemodynamic responses to acute threat (**Figure 3**) reflect
416 genuine surges in activation.

417

418

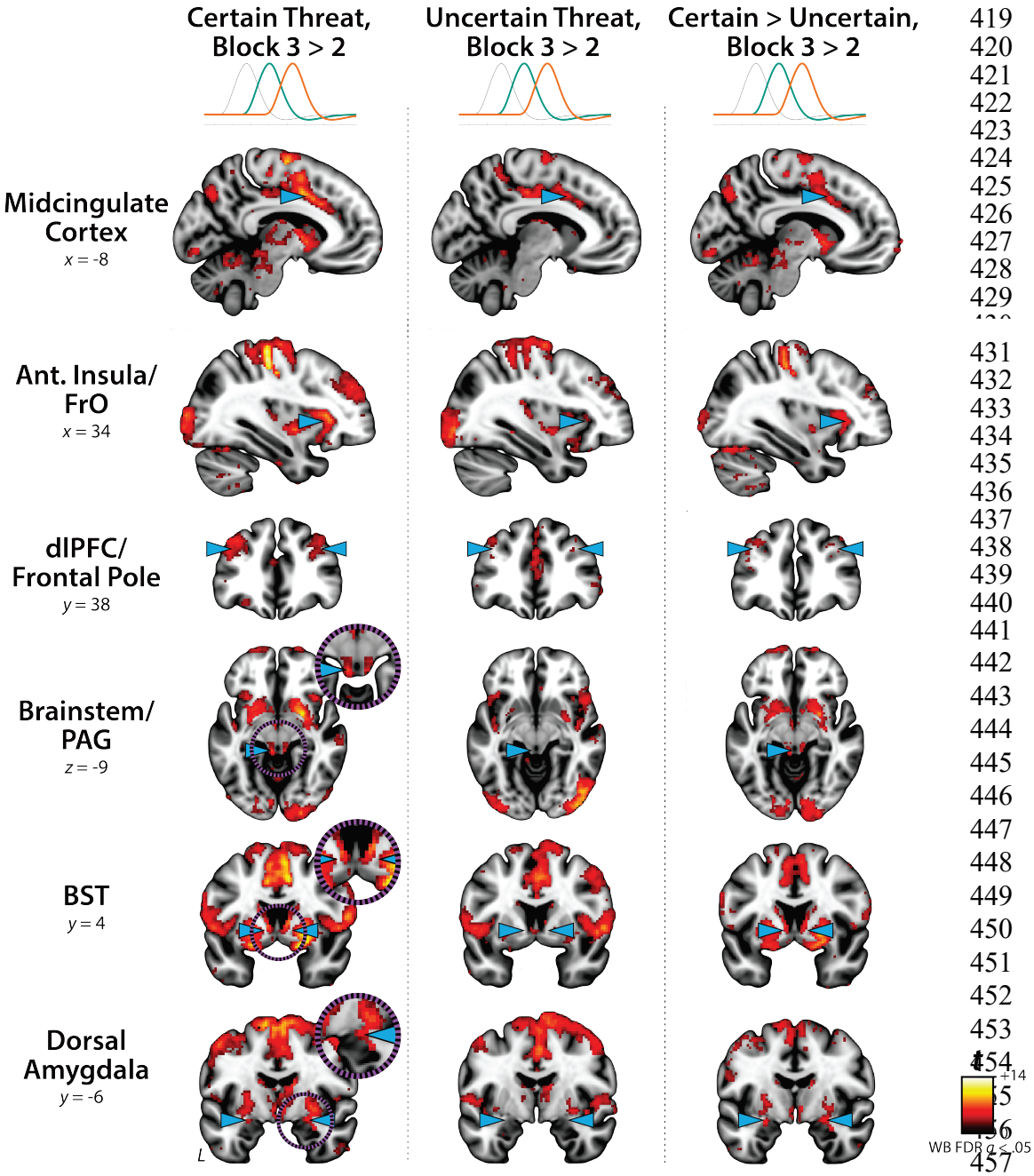

Supplementary Figure S5. Statistically interrogating time-varying responses to certain-and-imminent threat. Regions showing significant activation during the third 6.25-s block of certain-threat anticipation (*left column*) and uncertain-threat anticipation (*middle column*) compared to the second block (FDR q<0.05, whole-brain corrected). The *right column* depicts regions where surges in activation are significantly stronger for certain compared to uncertain threat (equivalent to testing the Block × Threat Certainty interaction). Results revealed significant activation surges in every key region except the PAG (*left column*), with a similar pattern evident for the between-moments comparison of certain to uncertain threat anticipation (*right column*). Note: 4-mm smoothing kernel. Abbreviations—Ant., anterior; BST, bed nucleus of the stria terminalis; dlPFC, dorsolateral prefrontal cortex; FDR, false discovery rate; FrO, frontal operculum; L, left; PAG, periaqueductal gray; t, Student's *t*-test; WB, whole-brain corrected.

472 **The BST and Ce show statistically indistinguishable neural dynamics**

473 Our approach also afforded a well-powered opportunity to revisit the functional architecture of the human
474 central extended amygdala (EAc), a macrocircuit encompassing the bed nucleus of the stria terminalis
475 (BST) and dorsal amygdala in the region of the central nucleus (Ce). There is widespread consensus that
476 the EAc plays a critical role in assembling defensive responses to a broad spectrum of threats and
477 contributes to the etiology of emotional illness[16, 18, 20, 21, 31, 39, 53]. Yet confusion persists about the respective
478 contributions of its two major subdivisions[42, 54]. Inspired by an earlier wave of loss-of-function studies in
479 rats[55], it is widely believed that these regions are dissociable, with the Ce mediating phasic responses to
480 certain-and-imminent harm and the BST mediating sustained responses to uncertain-or-remote danger[22,
481 37, 38, 56, 57]. This double-dissociation hypothesis has even been enshrined in the National Institute of Mental
482 Health's (NIMH) influential Research Domain Criteria (RDoC) framework as Acute Threat (*"fear"*) and
483 Potential Threat (*"anxiety"*)[34-36]. Yet a growing body of mechanistic and neuroimaging evidence motivates
484 the competing hypothesis that the BST and Ce both play a role in organizing phasic and sustained responses
485 to threat[18, 31, 32, 41, 42, 58, 59]. Because conventional voxelwise analyses do not permit inferences about regional
486 differences in activation, we used *a priori* probabilistic anatomical regions of interest (ROIs) to rigorously
487 assess these competing predictions (**Figure 4a**). Anatomical ROIs have the added advantage of providing
488 statistically unbiased effect-size estimates[60], in contrast to earlier work[32]. To maximize anatomical
489 resolution, mean activation was computed for bilateral BST and Ce ROIs using spatially unsmoothed data[61].
490 Hypothesis testing focused on regional responses to certain and uncertain threat, relative to their
491 respective reference conditions, using activation estimates from the Convolved Blocks model (**Figure 1c**).
492

493 As a precursor to hypothesis testing, we used one-sample Student's *t*-tests to confirm that the BST and Ce
494 are nominally engaged by anticipated threat ($p<0.05$, uncorrected). With one exception, results revealed
495 uniformly significant activation ($t(219)>2.08$, $p<0.04$). The Ce did not show significant evidence of

activation during the middle third of certain-threat anticipation ($t(219)=-0.40$, $p=0.69$). These observations indicate that both subdivisions of the EAc are sensitive to anticipated threat, regardless of the temporal certainty of encounters.

Next, we used a standard 2 (*Region:* BST, Ce) × 2 (*Threat Certainty:* Certain, Uncertain) × 3 (*Block:* Early, Middle, Late) repeated-measures GLM to formally test the double-dissociation hypothesis embodied in RDoC and other 'strict-segregation' models. None of the Regional effects were significant ($p>0.13$), including the conceptually critical Region × Threat Certainty × Block interaction ($F(2,438)=0.72$, $p=0.46$). Consistent with this, the BST and Ce showed negligible differences in activation during the second block (6.25-12.5 s) of uncertain-threat, an indicator of sustained activation, or the final block of certain-threat (12.5-18.75 s), an indicator of phasic surges in activation ($|t|(219)<1.31$, $p>0.18$; **Figure 4b-c** and **Supplementary Figure S6**). Frequentist effects were in the nil range ($|d|=0.03$-0.09) and Bayesian effects signaled moderate-to-strong evidence for the null ($BF_{10}=0.08$-0.17). Descriptively, participants were just as likely as not to show the RDoC-predicted regional differences; for example, 51% showed stronger BST-than-Ce activation during the second block of uncertain-threat anticipation. In short, we uncovered no evidence for the popular double-dissociation hypothesis, despite being powered to detect small regional differences in activation (**Supplementary Method**).

The central extended amygdala (EAc) exhibits context-dependent neural dynamics

On the other hand, GLM results did provide evidence that the EAc in aggregate—averaged across BST and Ce—shows context-dependent neural dynamics, as indexed by significant Block and Threat-Certainty × Block effects ($F(2,438)>5.18$, $p<0.01$). As shown in **Figure 4d**, polynomial-trend analyses revealed a marginally significant linear increase in EAc activation during uncertain-threat anticipation (*Linear:* $F(1,219)=3.58$, $p=0.06$; *Quadratic:* $F(1,219)=0.05$, $p=0.82$). In contrast, the EAc showed a pronounced

quadratic ('V-shaped') trend during certain-threat anticipation, manifesting as a dip in the middle third, followed by a surge of activation in the final third, when the threat encounter was most imminent (*Linear:* $F(1,219)=11.30$, $p<0.001$; *Quadratic:* $F(1,219)=10.38$, $p=0.001$).

Figure 4. The BST and Ce show statistically indistinguishable neural dynamics. a. *Probabilistic EAc anatomical ROIs.* The BST (*magenta*) and Ce (*yellow*) ROIs. **b. *Uncertain-threat anticipation, second convolved block.*** The BST and Ce show negligible differences in activation during the second block (6.25-12.5 s) of uncertain-threat anticipation **c. *Certain-threat anticipation, third convolved block.*** The BST and Ce show negligible differences during the final block (12.5-18.75 s) of certain-threat anticipation. **d. *The EAc shows context-dependent dynamics.*** In aggregate, the EAc evinced a marginally significant linear increase in EAc activation during uncertain-threat anticipation (*red*; p=0.06) and a pronounced quadratic ('V-shaped') trend during certain-threat anticipation (*orange*; p=0.001). Colored envelopes depict the SE. Note. Raincloud plots indicate the medians (*horizontal lines*), interquartile ranges (*boxes*), and smoothed density distributions. Whiskers depict 1.5× the interquartile range. Colored dots connected by gray lines indicate mean regional activation for each participant. Note: No spatial smoothing kernel was employed for ROI analyses. Abbreviations—BF, Bayes' factor; BST, bed nucleus of the stria terminalis; Ce, central nucleus of the amygdala; *d*, Cohen's *dz*; EAc, central extended amygdala; SE, standard error of the mean; *t*, Student's *t*-test.

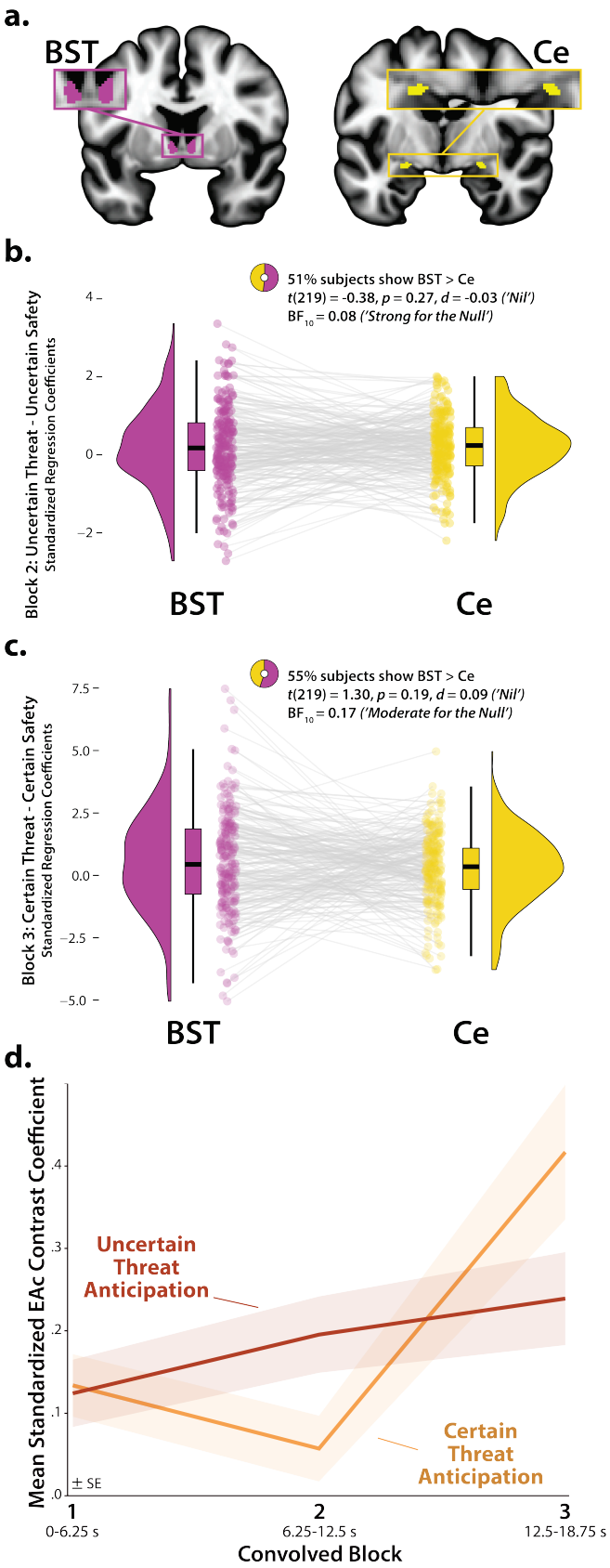

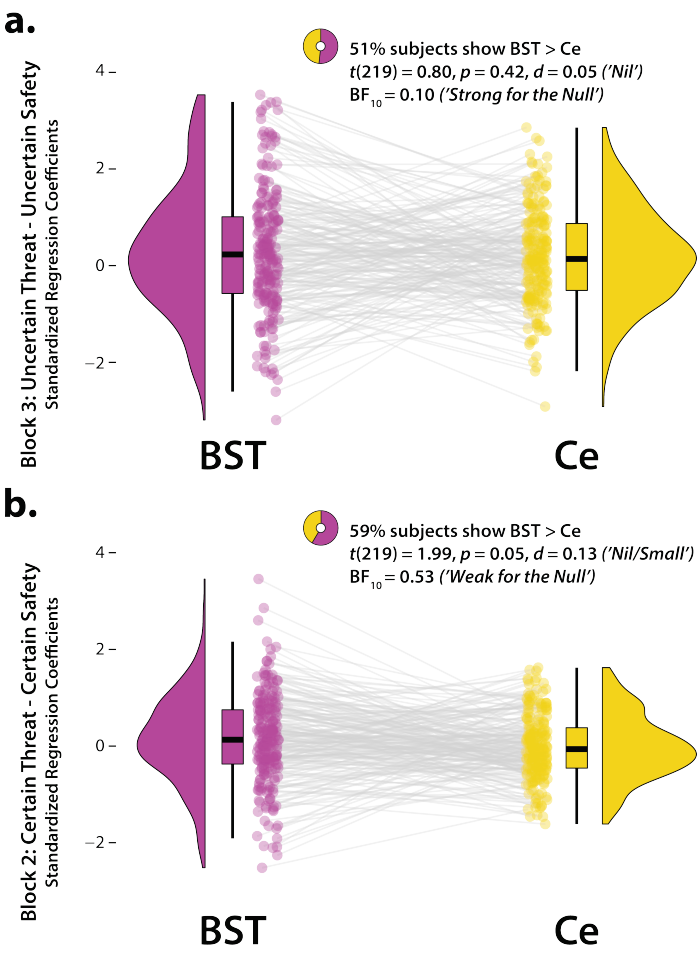

Supplementary Figure S6. The BST and Ce show statistically similar responses to uncertain- and certain-threat anticipation. a. *Uncertain-threat anticipation, third convolved block.* The BST and Ce show negligible differences in activation during the third block (12.5-18.75 s) of uncertain-threat anticipation **c. *Certain-threat anticipation, second convolved block.*** The BST and Ce show modest differences during the middle (6.25-12.5 s) of certain-threat anticipation. Raincloud plots indicate the medians (*horizontal lines*), interquartile ranges (*boxes*), and smoothed density distributions. Whiskers depict 1.5× the interquartile range. Colored dots connected by gray lines indicate mean regional for each participant. Note: No spatial smoothing kernel was employed for ROI analyses. Abbreviations—BF, Bayes' factor; BST, bed nucleus of the stria terminalis; Ce, central nucleus of the amygdala; *d*, Cohen's *dz*; EAc, central extended amygdala; *t*, Student's *t*-test.

652 **Momentary estimates of subjective distress show the same pattern of context-dependent**
653 **dynamics**

654 It is tempting to interpret our neuroimaging results in terms of conscious feelings—to infer that
655 participants experience a sustained state of elevated anxiety when the timing of threat encounters is
656 uncertain and a surge of fear in the seconds before certain encounters. Yet standard fMRI analyses cannot
657 address the momentary dynamics of threat-evoked distress, a limitation shared with other behavioral and
658 psychophysiological measures, and with mechanistic models in animals[1, 62]. Likewise, more intensive
659 continuous or intermittent ratings have the potential to fundamentally alter the nature of the experience[63,
660 64]. Here we used activation estimates derived from the Convolved Blocks model and an independently
661 trained and validated whole-brain 'signature' of subjective negative affect to unobtrusively probe the
662 momentary dynamics of threat-evoked feelings for the first time (**Figure 5a**)[65, 66]. Prior work demonstrates
663 that this signature is a sensitive indicator of distress elicited by a variety of noxious experiences—including
664 thermal and mechanical pain, unpleasant photographs, and aversive auditory stimuli—but is unrelated to
665 the intensity of feelings triggered by positive stimuli, indicating specificity[65]. Conceptually similar
666 multivoxel pattern analysis (MVPA) approaches have been successfully used in other areas of the cognitive
667 neurosciences; for example, to covertly decode the contents of working memory or the focus of selective
668 attention without disrupting on-going performance[66].
669

670 As a first step, we used one-sample Student's *t*-tests to confirm that the whole-brain signature—which was
671 trained using data time-locked to the *presentation* of noxious stimuli—is nominally sensitive to the
672 *anticipation* of multimodal threat ($p<0.05$, uncorrected). With one exception, results revealed robust
673 signature responses, signaling more intense negative affect ($t(219)>6.67$, $p<0.001$). Paralleling the EAc ROI
674 results, the signature did not show evidence of sustained distress in the middle third of certain-threat
675 anticipation ($t(219)=0.62$, $p=0.54$). Taken with our other measures of threat-elicited distress and arousal

(**Supplementary Figure S1**), these observations suggests that the signature is a valid index of threat-evoked anticipatory distress.

Next, we used a standard 2 (*Threat Certainty:* Certain, Uncertain) × 3 (*Block:* Early, Middle, Late) GLM to estimate momentary-by-moment fluctuations in distress across the two threat contexts. Consistent with our comparatively sparse retrospective ratings data (**Supplementary Figure S1**), results revealed significantly greater distress estimates, on average, when anticipating temporally uncertain threat encounters (*Threat Certainty:* $F(1,219)=8.47$, $p=0.004$; **Figure 5b**). The Block effect and Threat Certainty × Block interaction were also significant ($F(2,438)>19.34$, $p<0.001$). Although significant linear and quadratic polynomial trends were evident for both kinds of anticipated threat ($F(1,219)>5.00$, $p<0.03$), the V-shaped ('surge-trough-surge') quadratic effect was more than an order of magnitude stronger when anticipating certain-threat encounters (*Certain:* $p\eta^2=0.31$, $p=4.71 \times 10^{-19}$; *Uncertain:* $p\eta^2=0.02$, $p=0.02$; **Figure 5b**). In combination with the one-sample *t*-test results (see above), this indicates that the anticipation of temporally uncertain threat elicits a sustained state of heightened negative affect, whereas certain threat is associated with more complex distress dynamics, with negligible distress evident in the middle period and a phasic surge when threat is most imminent.

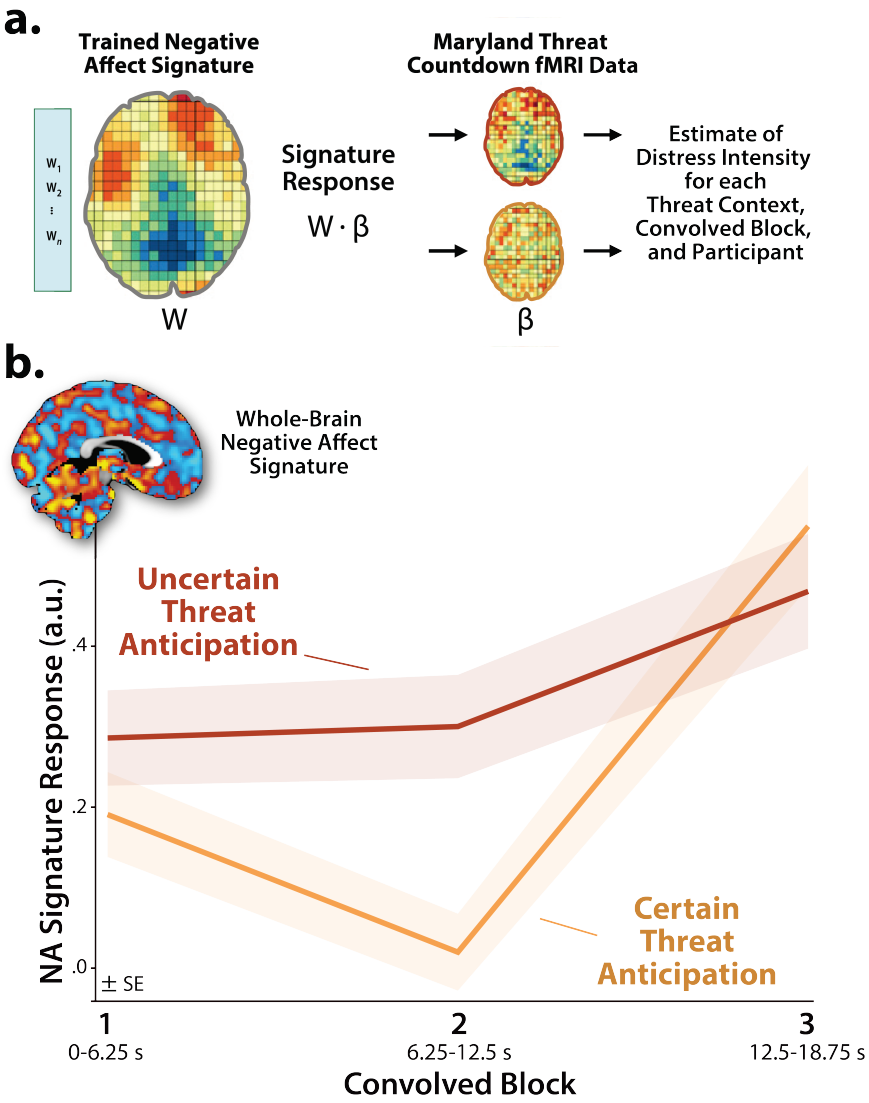

Figure 5. Using a multivoxel brain signature to probabilistically estimate dynamic fluctuations in threat-elicited distress. a. ***An independently trained and validated whole-brain signature of subjective negative affect was used to estimate threat-evoked distress.*** Čeko, Wager, and colleagues used machine-learning to develop a whole-brain 'signature'—a pattern of voxelwise weights (*w*)—that is predictive of negative affect intensity in unseen data across a variety of noxious stimuli[67]. In effect, the signature treats each voxel as a weighted source of information and the overall pattern as a collective 'best guess.' Computing the dot-product (•) between the pattern of weights (*W*) and voxelwise activation estimates (*β*) derived for the present sample using the Convolved Blocks model generates a signature response—a probabilistic estimate of distress intensity—for every combination of threat certainty, block, and participant. This made it possible to covertly estimate moment-by-moment fluctuations in threat-elicited distress and test whether distress dynamics are sensitive to the temporal certainty of threat encounters. **b.** ***Subjective distress shows context-dependent dynamics.*** The estimated intensity of distress was significantly greater, on average, when anticipating uncertain encounters with threat (p=0.004). Significant linear and quadratic polynomial trends were evident for both certain- and uncertain-threat anticipation (p<0.03), but the V-shaped quadratic effect was more than an order of magnitude stronger for certain threat (*Certain:* $p\eta^2$=0.31; *Uncertain:* $p\eta^2$=0.02). Inset depicts the whole-brain multivoxel signature of negative affect. Hot and cool colors indicate positive and negative signature weights, respectively. Colored envelopes depict the SE. Portions of this figure were reproduced with permission from Ref. [67]. Note: 4-mm smoothing kernel. Abbreviations—fMRI, functional magnetic resonance imaging; SE, standard error of the mean.

716 **DISCUSSION**
717
718 Since the time of Freud, the fear-versus-anxiety distinction has been a hallmark of prominent models of
719 emotion and emotional illness, including the DSM and RDoC[1, 2, 34-36, 68]. Despite the enormous significance
720 of threat-elicited emotions for public health, the neural systems underlying phasic responses to acute
721 danger and sustained responses to uncertain harm are contentious[1, 42, 54]. Some posit that *"fear"* and
722 *"anxiety"* are phenomenologically distinct states mediated by anatomically dissociable circuits[1, 16, 20, 37-40,
723 69], whereas others suggest that they are more biologically alike than different[31, 32]. Leveraging a relatively
724 large and ethnoracially diverse sample, translationally relevant fMRI paradigm, and theory-driven
725 hemodynamic modeling approach (**Figure 1**), our results demonstrate that the anticipation of temporally
726 certain and uncertain threat encounters recruit a remarkably overlapping distributed circuit, with
727 anatomical colocalization evident in many previously implicated regions (**Figures S2 and 3**). This shared
728 threat-anticipation circuit exhibits context-specific dynamics, evincing sustained levels of heightened
729 activation when threat encounters are uncertain and distal (**Figure 2**), and phasic surges in activation
730 when threat encounters are certain and imminent (**Figures 3 and S5**).

731

732 Among the regions highlighted by our results, the BST and Ce occupy center-stage in neurobiological
733 models of fear and anxiety. Yet their precise contributions remain a matter of active debate[42, 49, 70].
734 Leveraging anatomical ROIs and spatially unsmoothed data, our results demonstrate that the BST and Ce
735 exhibit statistically indistinguishable responses to anticipated threat—with frequentist effects in the nil
736 range ($|d|$=0.03-0.09) and Bayesian effects indicating moderate-to-strong evidence for the null hypothesis
737 (BF_{10}=0.08-0.17)—reinforcing the possibility that these two regions make broadly similar contributions to
738 human fear and anxiety (**Figure 4**)[32, 41, 59]. Both regions exhibit activation dynamics that run counter to
739 popular double-dissociation models, with the Ce showing sustained responses to uncertain-and-distal
740 threat and the BST showing phasic responses to acute threat.

741

742 Pathological fear and anxiety is defined, diagnosed, and treated on the basis of subjective symptoms, and
743 for many theorists, clinicians, and laypeople, conscious feelings are the defining feature of these emotions[1,
744 37, 71-74]. Yet standard fMRI analyses, like animal models, do not permit strong inferences about conscious
745 feelings. Here we used an independently trained and validated brain signature to unobtrusively decode the
746 momentary dynamics of threat-evoked distress for the first time[65]. Results indicated that uncertain-threat
747 anticipation is associated with a sustained state of elevated negative affect, whereas certain-threat
748 anticipation elicits more complex dynamics, with a phasic surge of distress evident just before threat
749 encounters (**Figure 5**). These observations reinforce the conclusion that human fear and anxiety, while
750 showing distinct patterns of context-dependent temporal dynamics, reflect the operation of a common
751 threat-anticipation circuit.

752

753 The core threat-anticipation circuit encompasses subcortical regions, such as the BST and Ce, that are
754 critical for assembling defensive responses to anticipated threat in animals[18, 41, 75]. But it also includes
755 frontocortical regions—including the MCC, AI/FrO, and dlPFC/FP—that have received less empirical
756 attention and are challenging or impossible to study in rodents[76-78]. These regions have traditionally been
757 associated with the controlled processing and regulation of emotion and cognition[44, 79-81] and more
758 recently implicated in the conscious experience of emotion[82]. The present findings extend past work
759 focused on descriptive hemodynamic modeling approaches in smaller samples[32, 33], and dovetail with
760 meta-analytic evidence that Pavlovian fear-conditioning tasks (the prototypical experimental model of
761 certain-and-imminent threat) and instructed threat-of-shock tasks (the prototypical experimental model
762 of uncertain threat) recruit strongly overlapping cortico-subcortical networks in humans, including the
763 BST[31, 83, 84].

764

The present results provide a keyboard of regions and activation-dynamics, setting the stage for identifying the functional-neuroanatomical combinations most relevant to the development of pathological fear and anxiety and to the efficacy of established therapeutics. Consider the widely prescribed anxiolytic, diazepam. As yet, the neurodynamic mechanisms that underlie the blockade of threat-elicited distress by diazepam and other benzodiazepine drugs remain unsettled. Does anxiolysis primarily reflect the dampening of sustained responses to uncertain threat in the Ce, as implied by recent work in mice[85], or widespread changes across multiple activation metrics, as implied by our signature results?

Our results add to a growing body of evidence that the BST and Ce, while certainly not interchangeable, are more functionally alike than different[41]. The two regions are characterized by broadly similar patterns of anatomical connectivity, cellular composition, neurochemistry, and gene expression[58]. Both are poised to trigger behavioral, psychophysiological, and neuroendocrine responses to threat via dense projections to downstream effector regions[58, 86]. Both are recruited by a broad spectrum of threatening and aversive stimuli[31-33, 41, 87]. Perturbation studies in rodents demonstrate that microcircuits within and between the Ce and BST are critical for orchestrating defensive responses to both acute and uncertain threats[18, 41, 48, 88-93]. While our understanding remains far from complete, this rapidly growing corpus of observations underscores the need to reformulate RDoC and other models that imply a strict segregation of certain and uncertain threat processing in the EAc. A key challenge for future research will be to determine whether our conclusions generalize to other types of threat (e.g., social), other kinds of threat uncertainty (e.g., probability, risk, ambiguity), and more naturalistic paradigms that span longer and more ecologically valid periods of threat anticipation[94]. Moving forward, an enhanced emphasis on computationally tractable paradigms has the potential to address fundamental questions about the function of the regions highlighted by our results and foster a common mathematical framework (*'lingua franca'*) for integrating research across assays, read-outs, and species[1, 95, 96]. The Ce and BST are complex and can be subdivided into multiple subdivisions, each containing intermingled cell types with distinct, even opposing functional

roles (e.g., anxiogenic vs. anxiolytic)[18, 41]. Animal models will be critical for identifying the molecules, cell types, and microcircuits governing activation dynamics in human neuroimaging studies[41].

In conclusion, the neural circuits recruited by temporally uncertain and certain threat are not categorically different, at least when viewed through the macroscopic lens of human neuroimaging. We see evidence of anatomical colocalization—*not* segregation—in the EAc and key frontocortical regions. This shared threat-anticipation circuit shows persistently elevated activation when anticipating temporally uncertain encounters with threat and an acute burst of activation in the moments before certain encounters. Subjective distress shows parallel dynamics. These observations provide a neurobiologically grounded framework for conceptualizing typical and pathological fear and anxiety in humans and lay the groundwork for more ambitious prospective-longitudinal, clinical, computational, and mechanistic work.

803 **REFERENCES**

804

805 1. Grogans, S.E., *et al.* The nature and neurobiology of fear and anxiety: State of the science and
806 opportunities for accelerating discovery. *Neuroscience & Biobehavioral Reviews* **151**, 105237 (2023).

807 2. APA. *Diagnostic and statistical manual of mental disorders, text revision (DSM-5-TR)* (American
808 Psychiatric Publishing, Washington, DC, 2022).

809 3. Salomon, J.A., *et al.* Disability weights for the Global Burden of Disease 2013 study. *Lancet Glob*
810 *Health* **3**, e712-723 (2015).

811 4. IMHE. *Anxiety disorders - Level 3 cause* (Institute for Health Metrics and Evaluation, Seattle, WA,
812 2024). https://www.healthdata.org/research-analysis/diseases-injuries-risks/factsheets/2021-anxiety-
813 disorders-level-3-disease

814 5. GBD 2021 Diseases and Injuries Collaborators. Global incidence, prevalence, years lived with
815 disability (YLDs), disability-adjusted life-years (DALYs), and healthy life expectancy (HALE) for 371
816 diseases and injuries in 204 countries and territories and 811 subnational locations, 1990-2021: a
817 systematic analysis for the Global Burden of Disease Study 2021. *The Lancet* **403**, 2133-2161 (2024).

818 6. Dieleman, J.L., *et al.* US health care spending by payer and health condition, 1996-2016. *JAMA* **323**,
819 863-884 (2020).

820 7. NCS-R. *National Comorbidity Study-Replication (NCS-R). Lifetime prevalence of DSM-IV/WMH-CIDI*
821 *disorders by sex and cohort [https://www.hcp.med.harvard.edu/ncs/ftpdir/NCS-*
822 *R_Lifetime_Prevalence_Estimates.pdf]* (2007). https://www.hcp.med.harvard.edu/ncs/ftpdir/NCS-
823 R_Lifetime_Prevalence_Estimates.pdf

824 8. The White House. *The White House report on mental health research priorities* (The White House
825 Office, Washington, DC, 2023).

826 9. U.S. Surgeon General. *Protecting youth mental health: The U.S. Surgeon General's advisory*
827 *[https://www.ncbi.nlm.nih.gov/books/NBK575984/]* (U.S. Department of Health and Human Services,
828 Washington, DC, 2021).

829 10. Mpofu, J.J.*, et al.* Overview and methods for the Youth Risk Behavior Surveillance System - United
830 States, 2021. *MMWR supplements* **72**, 1-12 (2023).
831 11. SAMHSA. *Key substance use and mental health indicators in the United States: Results from the 2022*
832 *National Survey on Drug Use and Health* (Center for Behavioral Health Statistics and Quality, Rockville, MD,
833 2023).
834 12. Batelaan, N.M.*, et al.* Risk of relapse after antidepressant discontinuation in anxiety disorders,
835 obsessive-compulsive disorder, and post-traumatic stress disorder: systematic review and meta-analysis
836 of relapse prevention trials. *BMJ* **358**, j3927 (2017).
837 13. Singewald, N., Sartori, S.B., Reif, A. & Holmes, A. Alleviating anxiety and taming trauma: Novel
838 pharmacotherapeutics for anxiety disorders and posttraumatic stress disorder. *Neuropharmacology* **226**,
839 109418 (2023).
840 14. Strawn, J.R., Lu, L., Peris, T.S., Levine, A. & Walkup, J.T. Pediatric anxiety disorders – what have we
841 learnt in the last 10 years? *Journal of Child Psychology and Psychiatry* **62**, 114-139 (2021).
842 15. Cuijpers, P.*, et al.* Absolute and relative outcomes of psychotherapies for eight mental disorders: a
843 systematic review and meta-analysis. *World Psychiatry* **23**, 267-275 (2024).
844 16. Tseng, Y.-T., Schaefke, B., Wei, P. & Wang, L. Defensive responses: behaviour, the brain and the body.
845 *Nature Reviews Neuroscience* **24**, 655-671 (2023).
846 17. Roelofs, K. & Dayan, P. Freezing revisited: coordinated autonomic and central optimization of threat
847 coping. *Nat Rev Neurosci* **23**, 568-580 (2022).
848 18. Moscarello, J.M. & Penzo, M.A. The central nucleus of the amygdala and the construction of defensive
849 modes across the threat-imminence continuum. *Nat Neurosci* **25**, 999-1008 (2022).
850 19. Mobbs, D., Headley, D.B., Ding, W. & Dayan, P. Space, time, and fear: Survival computations along
851 defensive circuits. *Trends in Cognitive Sciences* **24**, 228-241 (2020).
852 20. Davis, M., Walker, D.L., Miles, L. & Grillon, C. Phasic vs sustained fear in rats and humans: Role of the
853 extended amygdala in fear vs anxiety. *Neuropsychopharmacology* **35**, 105-135 (2010).

854 21. Tovote, P., Fadok, J.P. & Lüthi, A. Neuronal circuits for fear and anxiety. *Nat Rev Neurosci* **16**, 317-
855 331 (2015).
856 22. Grillon, C. Models and mechanisms of anxiety: evidence from startle studies. *Psychopharmacology*
857 **199**, 421-437 (2008).
858 23. Barlow, D.H. Unraveling the mysteries of anxiety and its disorders from the perspective of emotion
859 theory. *Am Psychol* **55**, 1247-1263 (2000).
860 24. Moberg, C.A., Bradford, D.E., Kaye, J.T. & Curtin, J.J. Increased startle potentiation to unpredictable
861 stressors in alcohol dependence: Possible stress neuroadaptation in humans. *Journal of Abnormal*
862 *Psychology* **126**, 441-453 (2017).
863 25. Hefner, K.R., Moberg, C.A., Hachiya, L.Y. & Curtin, J.J. Alcohol stress response dampening during
864 imminent versus distal, uncertain threat. *J Abnorm Psychol* **122**, 756-769 (2013).
865 26. Grillon, C., Ameli, R., Merikangas, K., Woods, S.W. & Davis, M. Measuring the time course of
866 anticipatory anxiety using the fear-potentiated startle reflex. *Psychophysiology* **30**, 340-346 (1993).
867 27. Grillon, C., Ameli, R., Foot, M. & Davis, M. Fear-potentiated startle: relationship to the level of
868 state/trait anxiety in healthy subjects. *Biol Psychiatry* **33**, 566-574 (1993).
869 28. Löw, A., Weymar, M. & Hamm, A.O. When threat is near, get out of here: Dynamics of defensive
870 behavior during freezing and active avoidance. *Psychol Sci* **26**, 1706-1716 (2015).
871 29. Wendt, J., Löw, A., Weymar, M., Lotze, M. & Hamm, A.O. Active avoidance and attentive freezing in
872 the face of approaching threat. *Neuroimage* **158**, 196-204 (2017).
873 30. Abend, R*., et al.* Threat imminence reveals links among unfolding of anticipatory physiological
874 response, cortical-subcortical intrinsic functional connectivity, and anxiety. *Neurobiol Stress* **16**, 100428
875 (2022).
876 31. Shackman, A.J. & Fox, A.S. Two decades of anxiety neuroimaging research: New insights and a look
877 to the future. *American Journal of Psychiatry* **178**, 106-109 (2021).

878 32. Hur, J., *et al.* Anxiety and the neurobiology of temporally uncertain threat anticipation. *Journal of*
879 *Neuroscience* **40**, 7949-7964 (2020).
880 33. Murty, D.V.P.S., Song, S., Surampudi, S.G. & Pessoa, L. Threat and reward imminence processing in
881 the human brain. *J Neurosci* **43**, 2973-2987 (2023).
882 34. NIMH. *Construct: Potential Threat ("Anxiety")* (2020).
883 https://www.nimh.nih.gov/research/research-funded-by-nimh/rdoc/constructs/potential-threat-
884 anxiety.shtml
885 35. NIMH. *Construct: Acute Threat ("Fear")* (2020). https://www.nimh.nih.gov/research/research-
886 funded-by-nimh/rdoc/constructs/acute-threat-fear.shtml
887 36. NIMH. *Negative valence systems: Workshop proceedings (March 13, 2011 – March 15, 2011; Rockville,*
888 *Maryland)* (2011). https://www.nimh.nih.gov/research/research-funded-by-nimh/rdoc/negative-
889 valence-systems-workshop-proceedings.shtml
890 37. LeDoux, J.E. & Pine, D.S. Using neuroscience to help understand fear and anxiety: A two-system
891 framework. *Am J Psychiatry* **173**, 1083-1093 (2016).
892 38. Avery, S.N., Clauss, J.A. & Blackford, J.U. The human BNST: Functional role in anxiety and addiction.
893 *Neuropsychopharmacology* **41**, 126-141 (2016).
894 39. Grupe, D.W. & Nitschke, J.B. Uncertainty and anticipation in anxiety: an integrated neurobiological
895 and psychological perspective. *Nat Rev Neurosci* **14**, 488-501 (2013).
896 40. Watson, D., Stanton, K. & Clark, L.A. Self-report indicators of negative valence constructs within the
897 research domain criteria (RDoC): A critical review. *J Affect Disord* **216**, 58-69 (2017).
898 41. Fox, A.S. & Shackman, A.J. The central extended amygdala in fear and anxiety: Closing the gap
899 between mechanistic and neuroimaging research. *Neuroscience Letters* **693**, 58-67 (2019).
900 42. Shackman, A.J., Grogans, S.E. & Fox, A.S. Fear, anxiety, and the functional architecture of the human
901 central extended amygdala. *Nature Reviews Neuroscience* (*in press*).

43. Grogans, S.E.*, et al.* Neuroticism/negative emotionality is associated with increased reactivity to uncertain threat in the bed nucleus of the stria terminalis, not the amygdala. *Journal of Neuroscience* (*in press*).

44. Hur, J.*, et al.* Anxiety-related frontocortical activity is associated with dampened stressor reactivity in the real world. *Psychological Science* **33**, 906-924 (2022).

45. Kim, H.C.*, et al.* Acute nicotine abstinence amplifies subjective withdrawal symptoms and threat-evoked fear and anxiety, but not extended amygdala reactivity. *PLoS One* **18**, e0288544 (2023).

46. Daldrup, T.*, et al.* Expression of freezing and fear-potentiated startle during sustained fear in mice. *Genes Brain Behav* **14**, 281-291 (2015).

47. Miles, L., Davis, M. & Walker, D. Phasic and sustained fear are pharmacologically dissociable in rats. *Neuropsychopharmacology* **36**, 1563-1574 (2011).

48. Lange, M.D.*, et al.* Cannabinoid CB1 receptors in distinct circuits of the extended amygdala determine fear responsiveness to unpredictable threat. *Mol Psychiatry* **22**, 1422-1430 (2017).

49. Wang, L., Tseng, Y.-T., Schaefke, B., Wei, P. & He, S. Reply to 'Fear, anxiety and the functional architecture of the human central extended amygdala'. *Nature Reviews Neuroscience* (*in press*).

50. Nichols, T., Brett, M., Andersson, J., Wager, T. & Poline, J.B. Valid conjunction inference with the minimum statistic. *Neuroimage* **25**, 653-660 (2005).

51. Sokolov, E.N., Spinks, J.A., Näätänen, R. & Lyytinen, H. *The orienting response in information processing* (Lawrence Erlbaum Associates, Mahwah, NJ, 2002).

52. Menon, V. Salience network. in *Brain Mapping* (ed. A.W. Toga) 597-611 (Academic Press, Cambridge, MA, 2015).

53. Hur, J., Stockbridge, M.D., Fox, A.S. & Shackman, A.J. Dispositional negativity, cognition, and anxiety disorders: An integrative translational neuroscience framework. *Progress in Brain Research* **247**, 375-436 (2019).

54. Daniel-Watanabe, L. & Fletcher, P.C. Are fear and anxiety truly distinct? *Biological Psychiatry Global Open Science* **2**, 341-349 (2022).

927 55. Davis, M. Neural systems involved in fear and anxiety measured with fear-potentiated startle. *Am*
928 *Psychol* **61**, 741-756 (2006).
929 56. Klumpers, F., Kroes, M.C.W., Baas, J. & Fernandez, G. How human amygdala and bed nucleus of the
930 stria terminalis may drive distinct defensive responses. *J Neurosci* **37**, 9645-9656 (2017).
931 57. Öhman, A. Fear and anxiety: Overlaps and dissociations. in *Handbook of emotions* (ed. M. Lewis, J.M.
932 Haviland-Jones & L.F. Barrett) 709-728 (Guilford, New York, NY, 2008).
933 58. Fox, A.S., Oler, J.A., Tromp, D.P., Fudge, J.L. & Kalin, N.H. Extending the amygdala in theories of threat
934 processing. *Trends Neurosci* **38**, 319-329 (2015).
935 59. Gungor, N.Z. & Paré, D. Functional heterogeneity in the bed nucleus of the stria terminalis. *Journal*
936 *of Neuroscience* **36**, 8038-8049 (2016).
937 60. Poldrack, R.A.*, et al.* Scanning the horizon: towards transparent and reproducible neuroimaging
938 research. *Nature Reviews Neuroscience* **18**, 115-126 (2017).
939 61. Tillman, R.M.*, et al.* Intrinsic functional connectivity of the central extended amygdala. *Human Brain*
940 *Mapping* **39**, 1291-1312 (2018).
941 62. Poldrack, R.A. Inferring mental states from neuroimaging data: from reverse inference to large-scale
942 decoding. *Neuron* **72**, 692-697 (2011).
943 63. Ruef, A.M. & Levenson, R.W. Continuous measurement of emotion: The affect rating dial. in
944 *Handbook of emotion elicitation and assessment.* (ed. J.A. Coan & J.J.B. Allen) 286-297 (Oxford University
945 Press, New York, NY, 2007).
946 64. Lieberman, M.D. Searching for implicit emotion regulation. in *The nature of emotion. Fundamental*
947 *questions* (ed. A.S. Fox, R.C. Lapate, A.J. Shackman & R.J. Davidson) 169-172 (Oxford University Press, New
948 York, NY, 2018).
949 65. Čeko, M., Kragel, P.A., Woo, C.-W., López-Solà, M. & Wager, T.D. Common and stimulus-type-specific
950 brain representations of negative affect. *Nature Neuroscience* **25**, 760-770 (2022).

66. Peelen, M.V. & Downing, P.E. Testing cognitive theories with multivariate pattern analysis of neuroimaging data. *Nat Hum Behav* **7**, 1430-1441 (2023).

67. Ceko, M., Kragel, P.A., Woo, C.W., Lopez-Sola, M. & Wager, T.D. Common and stimulus-type-specific brain representations of negative affect. *Nat Neurosci* **25**, 760-770 (2022).

68. Freud, S., Strachey, J., Freud, A., Rothgeb, C.L. & Richards, A. *The standard edition of the complete psychological works of Sigmund Freud, Volume 20 (1925-1926): An autobiographical study, inhibitions, symptoms and anxiety, the question of lay analysis and other works* (Hogarth Press, London, 1959).

69. Somerville, L.H.*, et al.* Interactions between transient and sustained neural signals support the generation and regulation of anxious emotion. *Cereb Cortex* **23**, 49-60 (2013).

70. Blanchard, D.C. & Canteras, N.S. In search of the behavioral and neural basis for differentiating fear and anxiety. *Biological Psychiatry: Global Open Science* **4**, 394-395 (2024).

71. Fox, A.S., Lapate, R.C., Shackman, A.J. & Davidson, R.J. *The nature of emotion. Fundamental questions* (Oxford University Press, New York, NY, 2018).

72. LeDoux, J.E. Rethinking the emotional brain. *Neuron* **73**, 653-676 (2012).

73. Taschereau-Dumouchel, V., Michel, M., Lau, H., Hofmann, S.G. & LeDoux, J.E. Putting the "mental" back in "mental disorders": a perspective from research on fear and anxiety. *Mol Psychiatry* **27**, 1322-1330 (2022).

74. Mobbs, D.*, et al.* Viewpoints: Approaches to defining and investigating fear. *Nature Neuroscience* **22**, 1205-1216 (2019).

75. Oler, J.A., Fox, A.S., Shackman, A.J. & Kalin, N.H. The central nucleus of the amygdala is a critical substrate for individual differences in anxiety. in *Living without an amygdala* (ed. D.G. Amaral & R. Adolphs) 218-251 (Guilford, NY, 2016).

76. Carlén, M. What constitutes the prefrontal cortex? *Science* **358**, 478-482 (2017).

77. Roberts, A. Prefrontal regulation of threat-elicited behaviors: A pathway to translation. *Annual Review of Psychology* **71**, 357-387 (2020).

976 78. Preuss, T.M. Do rats have prefrontal cortex? The Rose-Woolsey-Akert program reconsidered. *J Cog*
977 *Neurosci* **7**, 1-24 (1995).
978 79. Shackman, A.J.*, et al.* The integration of negative affect, pain and cognitive control in the cingulate
979 cortex. *Nat Rev Neurosci* **12**, 154-167 (2011).
980 80. Bo, K.*, et al.* A systems identification approach using Bayes factors to deconstruct the brain bases of
981 emotion regulation. *Nat Neurosci* **27**, 975-987 (2024).
982 81. Qi, S.*, et al.* How cognitive and reactive fear circuits optimize escape decisions in humans. *Proc Natl*
983 *Acad Sci U S A* **115**, 3186-3191 (2018).
984 82. LeDoux, J.E. Thoughtful feelings. *Current Biology* **30**, R619-R623 (2020).
985 83. Fullana, M.A.*, et al.* Neural signatures of human fear conditioning: An updated and extended meta-
986 analysis of fMRI studies. *Molecular Psychiatry* **21**, 500-508 (2016).
987 84. Chavanne, A.V. & Robinson, O.J. The overlapping neurobiology of adaptive and pathological anxiety:
988 a meta-analysis of functional neural activation. *American Journal of Psychiatry* **178**, 156-164 (2021).
989 85. Griessner, J.*, et al.* Central amygdala circuit dynamics underlying the benzodiazepine anxiolytic
990 effect. *Mol Psychiatry* **26**, 534-544 (2021).
991 86. Davis, M. & Whalen, P.J. The amygdala: vigilance and emotion. *Mol Psychiatry* **6**, 13-34 (2001).
992 87. Meyer, C., Padmala, S. & Pessoa, L. Dynamic threat processing. *J Cogn Neurosci* **31**, 522-542 (2019).
993 88. Zhu, Y.*, et al.* Distinct circuits from the central lateral amygdala to the ventral part of the bed nucleus
994 of stria terminalis regulate different fear memory. *Biol Psychiatry* **95**, 732-744 (2024).
995 89. Pomrenze, M.B.*, et al.* Dissecting the roles of GABA and neuropeptides from rat central amygdala
996 CRF neurons in anxiety and fear learning. *Cell Rep* **29**, 13-21 e14 (2019).
997 90. Chen, W.H., Lien, C.C. & Chen, C.C. Neuronal basis for pain-like and anxiety-like behaviors in the
998 central nucleus of the amygdala. *Pain* **163**, e463-e475 (2022).
999 91. Ren, J.*, et al.* A distinct metabolically defined central nucleus circuit bidirectionally controls anxiety-
000 related behaviors. *J Neurosci* **42**, 2356-2370 (2022).

001 92. Ressler, R.L., Goode, T.D., Evemy, C. & Maren, S. NMDA receptors in the CeA and BNST differentially
002 regulate fear conditioning to predictable and unpredictable threats. *Neurobiology of Learning and Memory*
003 **174**, 107281 (2020).
004 93. Pomrenze, M.B.*, et al.* A corticotropin releasing factor network in the extended amygdala for anxiety.
005 *J Neurosci* **39**, 1030-1043 (2019).
006 94. Mobbs, D.*, et al.* Promises and challenges of human computational ethology. *Neuron* **109**, 2224-2238
007 (2021).
008 95. Drzewiecki, C.M. & Fox, A.S. Understanding the heterogeneity of anxiety using a translational
009 neuroscience approach. *Cognitive, affective & behavioral neuroscience* **24**, 228-245 (2024).
010 96. Holley, D., Varga, E.A., Boorman, E.D. & Fox, A.S. Temporal dynamics of uncertainty cause anxiety
011 and avoidance. *Computational Psychiatry* **8**, 85-91 (2024).

012
013